

Aerothermodynamic Study on Clefted Wing

Amala A^{AB*}, Srinivasa Rao P^{AB}

^ADepartment of Aeronautical Engineering, Vardhaman College of Engineering, Shamshabad, Hyderabad, India
^BGews Technical Foundations, Hyderabad, India

Accepted 10 January 2014, Available online 01 February 2014, **Special Issue-2, (February 2014)**

Abstract

The UAVs in modern days are subjected to a large operating ranges and wide environmental conditions. The tremendous changes in the wing design of UAVs in recent times lead to high lift generating wings. A clefted wing with NACA 2412 airfoil is designed and tested in the wind tunnel under subsonic flow conditions. The investigations revealed that a considerable increase in the aerodynamic performance of the wing and it can be achieved with the Clefted wing under subsonic flow conditions. In comparison with the wing section of NACA2412 clefted wing is generating improved lift. However the aerodynamic heating is going to limit the flight conditions considerably. In this paper we study numerically the thermal stability of the clefted wing under both transonic and supersonic flow conditions. The thermal stresses generated under subsonic flows are compared with the experimental values and the supersonic flight thermal behaviour is estimated using CFD. The heat transfer analysis is performed for $1 \times 10^8 < \text{Grashoff Number (Gr)} < 5 \times 10^8$ on the wing leading edge. Geometric effects surrounding the leading edge are investigated in order to understand its influence on heat transfer and thermal stresses. It is found that the internal thermal stress distribution is finely depends upon Gr, as the increase in the depth of the cleft is increasing. It is also found that the clefted wing is more sensitive for the thermal loads than the normal NACA series wings.

Keywords: Wing, Airfoil Analysis, UAVs and Low Reynolds Number flows

1. Introduction

The interests in small unmanned aerial vehicles (UAV's) are increased greatly in the past decade. The size of such vehicles and the velocity at which they operate in are low Mach number flight regime. In this range the wings aerodynamics performances can deteriorate rapidly as the Mach number decreases. So the clefted wing is optimized to prevent stall and to improve aerodynamics performance. The airfoil in many respects is the heart of the airplane. The airfoil affects the cruise speed, takeoff and landing distance, stall speed, handling qualities and overall aerodynamics efficiency during all phases of flight. Methods have been developed for designing an airfoil such that the pressure differential between the top and bottom of the airfoil quickly reaches a maximum value attainable without airflow separation toward the rear of the airfoil, various pressure recovery schemes are employed to prevent separation near the trailing edge. These airfoil optimization techniques result in airfoil with substantial pressure differentials over a much greater percent of chord than a classical airfoil. The researchers reported an improvement for aerodynamics performance and increase of angle of attack. This permits a reduced wing area for a required amount of lift. We experiment for two different wings by inspired in the humpback whale flipper. In this

work we performance the numerical simulation of the setup used for the experimental study.

Our goal with this work is to increase the knowledge about these higher mach numbers flows which will be useful for the design of more efficient UAV's Wings.

2. Simulation Methodology

All the figures must be placed in the column wise,

2.1 Governing Equations

Integral form of the Continuity equation

$$\frac{\partial}{\partial t} \iiint_V \rho dv + \oint_S \rho V \cdot dS = 0 \quad (1)$$

Integral form of the Momentum equation

$$\frac{\partial}{\partial t} \iiint_V \rho V dv + \oint_S (\rho V \cdot dS) V = - \oint_S P dS + \iiint_V \rho f dv + F_{vis} \quad (2)$$

Integral form of the Energy equation

$$\iiint_V \rho q dv + Q_{vis} - \oint_S p V \cdot dS + \iiint_V \rho (f \cdot V) dv + W_{vis}$$

*Corresponding author: **Amala A**

$$= \frac{\partial}{\partial t} \iiint_V \rho \left(e + \frac{V^2}{2} \right) dV + \iint_S \rho \left(e + \frac{V^2}{2} \right) V \cdot dS \quad (3)$$

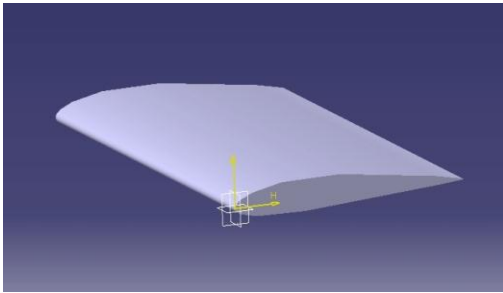


Fig. 1 NACA 2412 Normal Wing

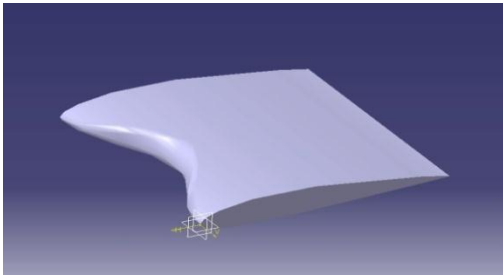


Fig. 2 NACA 2412 Clefted Wing

NACA 2412 is commonly used airfoil in many of the more successful models that were altered to study and analyze the behavior of entirely new air foil shapes. It has 1.92% camber compared to the clark Y's 3.43%.both are 12% or very close to it (11.7 for Clark Y). The clark Y should have the advantage in lower landing speeds and ease of building.

Both airfoils are 2m long and the chord length of 1m, the maximum chamber location from leading edge is 0.4, maximum thickness is 0.12. Maximum camber is 0.02. mach number for the experiment was 0.4 to 0.6.To maintain this values in our numerical simulation the pressure at the inflow boundary is pressure far field which corresponds to a temperature is 300⁰k. The front of the airfoil is defined by a leading edge radius that is tangent to the upper and lower surfaces. An airfoil designed to operate in supersonic flow will have a sharp or nearly sharp leading edge to prevent a drag producing bow shock.

The chord of the airfoil is the straight line from the leading edge to the trailing edge. It is very difficult to build a perfectly sharp trailing edge, so most airfoils have a blunt trailing edge with some small finite thickness. Camber refers to the curvature characteristics of most airfoils. The mean chamber line is the line equidistant from the upper and lower surfaces.

Unsteady Reynolds-Averaged Navier-Stokes (RANS) simulation (Paterson et al. 2003) on airfoil baseline foil with and without equally spaced tubercles showed flow-separation patterns and surface pressure to be dramatically altered by the tubercles. For regions downstream of the tubercle crest, separation was delayed almost to the trailing edge. This appears to be due to an increase in pressure on the suction side, which locally reduces the adverse pressure gradient. The tubercles generate

separated, chord wise vortices in the troughs. Flow strikes the surface of the trough obliquely and is sheared to the trough's center to generate the vortices. These vortices are convected along the chord. The span wise arrangement of the vortices is in a pair on each side of the tubercle's crest with opposite spins (Hansen et al. 2010).

The graphs must be properly drawn in MS excel. Please note that all the legends should be drawn in the MS excel single file. They are not to be inserted in MS Word which will affect the formatting of the template. Care should also be taken to keep the font as Times New Roman. As the default font in Excel is Calibri. So the graphs by default take it. The authors are required to keep the font as Times New Roman.

2.2 Boundary Conditions

The mesh generation was done using the software Gambit 3.1. The mesh elements are tetrahedral on the surface and the the wing aspect ratio is 5. All the dimensions are scaled with a scaling factor 1:15. Both the clefted wing and the normal wing sections are tested for the consistency in the mesh and the mesh distribution has been normalized using smoothing methods.

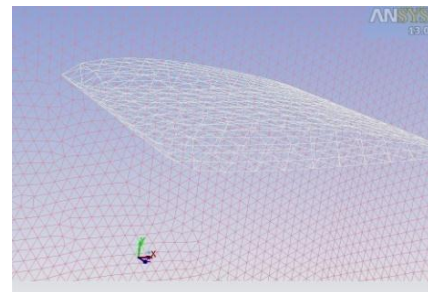


Fig.3. Mesh of Normal Wing



Fig.4. Mesh of Clefted Wing

Table 1 Boundary Conditions

Boundaries	Type and Values
Pressure	Pressure far field, Atm
Airfoil	Wall
Temperature	300 K
Mach number	0.6-1.2 M
Operating condition	101325pascal
Gauge pressure	0 bar

3. Results and discussion

The presentation of results is followed case wise starting from the initial velocities and the far field pressures. The comparison between the numerical results and experiments is presented. The results clearly shows that the contrast between the two wing geometries that are considered in the research. The wind tunnel test results are in good agreement with CFD predicted values. The turbulence model followed is Large Eddy Simulation (LES) which is numerically able to predict the nature of drag on the new air-foil and the predicted turbulent vortices are in well comparison with the experimental results.

The vortices produced from the tubercles were considered to re-energize the boundary layer by carrying high-momentum flow close to the flipper's surface. In addition, the aerodynamics is improved by confining separation to the tip region. A separate computational model (Unsteady RANS using the k-ε and Spalart-Allmaras turbulence models) which also replicated geometry previously tested in a wind tunnel found that tubercles delay stall by causing a greater portion of the flow to remain attached on a flipper with tubercles as compared to a flipper without tubercles, and also found that the attached flow was localized behind the crests of the tubercle.

3.1 Case of MACH 0.6

For a clefted wing, the Mach number increases at the clefted region as shown in fig.5 and remains constant throughout the flight, but in case of normal wing the Mach number decrease gradually and flow of air distributes in form of elliptical shape. In clefted wing the static pressure distribution at the leading edge is more compare to the normal wing and remains constant. In clefted wing due to maximum static pressure produced, the lift efficiency will be more. The temperature distribution over the both wings will be at study conditions.

For regions downstream of the turbulence, separation was delayed almost to the trailing edge. This appears to be due to an increase in pressure on the suction side, which locally reduces the adverse pressure gradient. For a clefted wing, the pressure increases at the clefted region (fig.4), but in case of normal wing the pressure decrease gradually and flow of air distributes in form of elliptical shape.

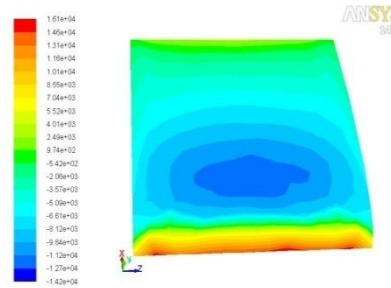


Fig.7. Pressure Contour of Normal Wing

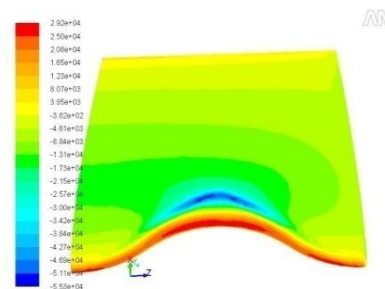


Fig.8. Pressure Contour of Clefted Wing

On the clefted wing the static pressure distribution at the leading edge is more when compared to the normal wing and remains constant. Under such conditions on the clefted wing due to maximum static pressure produced, the lift efficiency will be more.

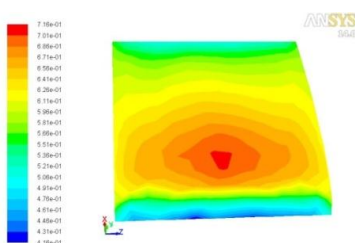


Fig.5 Mach contour Normal Wing

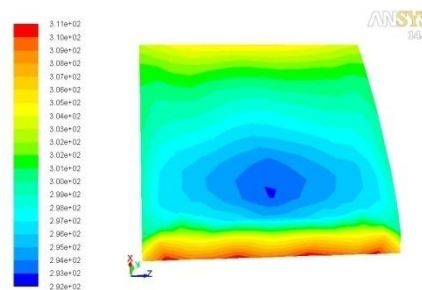


Fig.9 Temperature contour normal wing

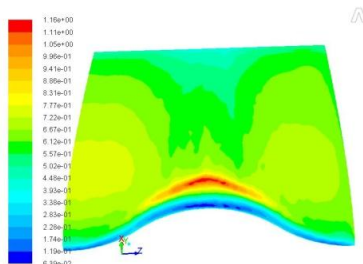


Fig.6 Mach contour Clefted Wing

The temperature distribution over the both wings found to be interesting as a matter of importance under study conditions. For a clefted wing, the temperature found to be increases at the clefted region (fig.5) and remains constant throughout the flight, but in case of normal wing temperature gradually increases and flow of air distributes in form of elliptical shape. For clefted wing the Temperature is varying less when compare with the normal wing.

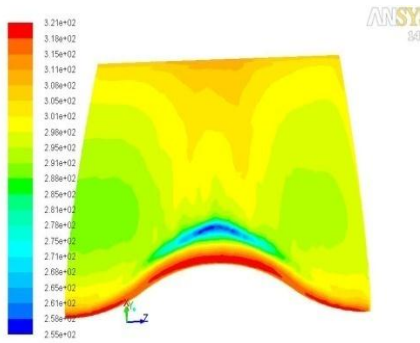


Fig.10 Temperature contour normal wing

3. 2 Case of MACH 1.2

The pressure and temperature varies due to change in Mach number. For a clefted wing, the Mach number increases at the clefted region (fig.6) and remains constant throughout the flight, but in case of normal wing the Mach number decrease gradually and flow of air distributes in form of elliptical shape. Flow visualization in the contours show significant differences in the flow field surrounding foils with protuberances as opposed to the baseline leading edge. The presence of protuberances along the leading edge effectively creates a varying leading edge sweep angle along the span. This in turn introduces span-wise flow along the leading edge in the form of stream-wise vortices. These vortices result in low pressures along the foil surface and are responsible for generating added lift past the stall angle of the baseline. This kind of effect is also seen in delta wings, in which vortices are generated along the edge of the wing creating a low pressure system on the surface of the wing.

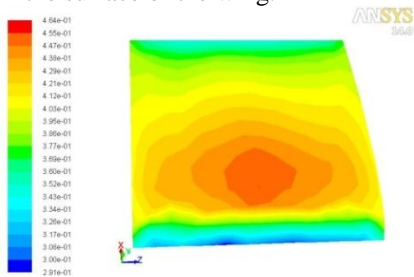


Fig.11 Mach number contour of Normal Wing

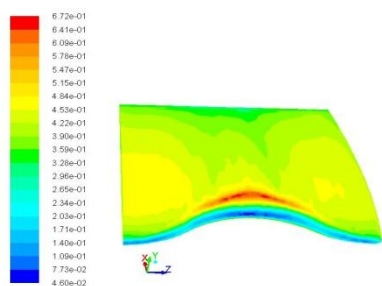


Fig.12 Mach number contour of Clefted Wing

Pressure contour of 0.4 for a clefted wing, the pressure increases at the clefted region (fig 7), but in case of normal wing the pressure decrease gradually and flow of air distributes in form of elliptical shape. In clefted wing the

static pressure distribution at the leading edge is more compare to the normal wing and remains constant. In clefted wing due to maximum static pressure produced, the lift efficiency will be more.

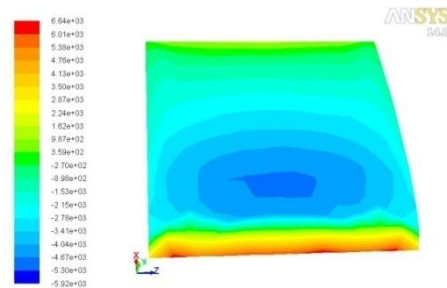


Fig.13 Pressure distribution of Normal Wing

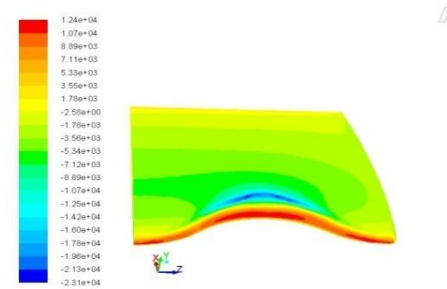


Fig.14 Pressure distribution of Clefted Wing

The temperature distribution over the both wings will be at study conditions. For clefted wing the Temperature is varying less when compare with the normal wing, because of less temperature that we can reduce the aerodynamic heating. Temperature is less in clefted wing when compare with the normal wing. It produces much less heating at subsonic speeds but becomes more important at supersonic speeds. The cleft of bodies and leading edges of wings for high speed flight are being blunted in order to reduce the transfer of heat in this region. The clefted is beneficial, regardless of whether the flow in the boundary layer is laminar or turbulent. At the high Reynolds numbers the turbulent heat transfer in the stagnation region is greater for turbulent than for laminar flow.

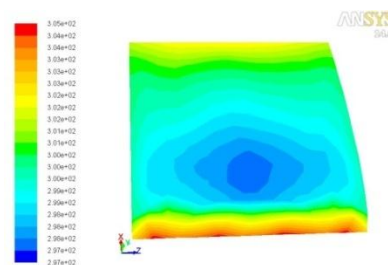


Fig.15 Temperature of Normal Wing

Graphs 16 shows that the marginally large amount of lift is produced due to clefted wing compared to normal wing. In clefted wing, the Mach number increases at the position of clefted and remains constant but in normal wing the Mach number gradually decreases. Normally, flow attachment and lift and drag considerations inhibit the capabilities of the control surface.

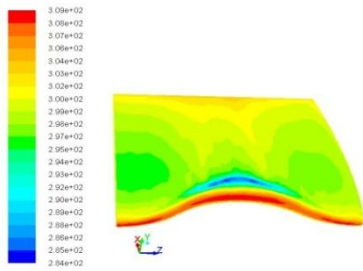


Fig.16 Temperature of Clefted Wing

It can be observed that the flow at the starting of the wing section is normal compared to the clefted wing and the gradual departure of the fluid over the wing seems to follow the nearly un-separated flow and through which the greater lift can be obtained over long range flow speeds.

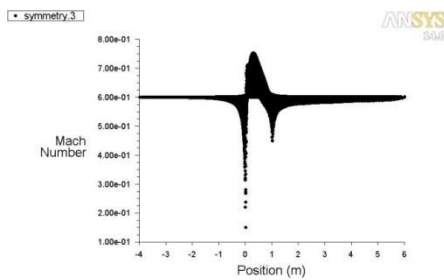


Fig.17 graph of mach number

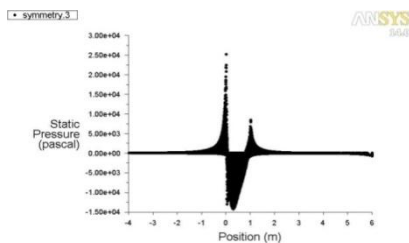


Fig.18 graph of static pressure

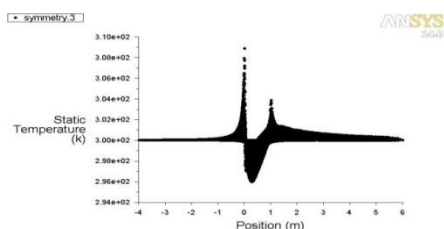


Fig.19 graph of temperature

Conclusions

The most important findings are reported and summarized in the following manner:

- The low Reynolds number flows are influenced by the flow separation which is observed in the clefted wings. The outboard section, dominated by lower Reynolds regime displays a leading edge type of separation; the inboard section display trailing edge separation.

- The higher aerodynamic performance for the wing is due to the presence of stream-wise vortices originated by the clefts. The reason why it improves the aerodynamics is twofold. In first place the vortices carry momentum to the boundary layer delaying the trailing-edge separation; secondly these vortices confine the leading edge separation to the tip region.
- The LES turbulence model was successfully used to determine the clefted wing aerodynamics in the range of low Reynolds numbers.

References

Mueller1, T.J. and DeLaurie, J.D., Aerodynamics of Small Vehicles, Annu. Rev. Fluid Mech, Vol.35, 2003, pp. 89 –111.

D. S. Miklosovic, M. M. Murray, L. E. H. and Fish, F. E., Leading-edge tubercles delay stall on humpback whale (Megaptera novaeangliae) flipper, Physics of Fluids, Vol. 16, 2004, pp. 39 – 42.

Becky L. Woodward, J. P. W. and Fish, F. E., Morphological Specializations of Baleen Whales Associated with Hydrodynamic Performance and Ecological Niche, Journal of morphology, Vol. 267, 2006, pp. 1284 – 1294.

Spalart, P., Strategies for turbulence modelling and simulations, International Journal of Heat and Fluid Flow, Vol. 21, 2000, pp. 252 – 263.

L. S. Hedges, A. T. and Spalart, P., Detached-Eddy Simulations Over a Simplified Landing Gear, Journal of Fluids Engineering, Vol. 124, 2002, pp. 413 – 423.

Scott Morton, James Forsythe, A. M. and Hajek, D., Detached-Eddy Simulations and Reynolds-Averaged Navier-Stokes Simulations of Delta Wing Vortical Flowfields, Journal of Fluids Engineering, Vol. 124, 2002, pp. 924 – 932.

Andrei Travin, Michael Shur, M. S. and Spalart, P., Detached-Eddy Simulations Past a Circular Cylinder, Flow, Turbulence and Combustion, Vol. 63, 2000, pp. 293 – 313.

Spalart P., Young-Person’s Guide to Detached-Eddy Simulation Grids, NASA/CR-2001-211032, 2001.

Hugo T. C. Pedro_ and Marcelo H. Kobayashi, Numerical Study of stall delay on humpback whale flippers, 46th AIAA Aerospace Sciences Meeting and Exhibit, 7-10 January 2008, Reno, Nevada

J. corneli, V.Ettinger, W. Baumgart, (2004), Thermal analysis ,an Unique Fingerprint of a melt ,66th World Foundry Congress 6-9 , pp. 743-756.

Seidu, S.O (2008). Influence of Inoculant’s type on thermal analysis parameters of ductile irons, 4th international conference, Galati, Romania, pp. 237-241.

M. Chisamera, S. Stan, I. Riposan, E. Stefan, G. Costache, (2007), Thermal analysis of Inoculated Grey Cast Irons, UGALMAT, Galati, Technologiisi Materiale Avansate, University press, Vol.1, pp.17-23.

Seidu, S.O., Riposan, I, (2011), Thermal analysis of inoculated ductile irons University Politehnica of Bucharest Scientific Bulletin, Series B, Vol. 73, Iss.2, Romania

Y. Gunay, S. Decirmenci, I. Metan, B. Sirin, (2004), The Application of Adaptive Thermal Analysis System (ATAS) on Grey and Ductile Iron Production, 66th World Foundry Congress, 06-09.09., Istanbul, Turkey.